Matrices used for fast atom bombardment (FAB) were 3-nitrobenzyl alcohol, 5:1 dithiothreitol/dithioerythreitol, and 2:1 thioglycerol/glycerol and were obtained from Aldrich. The $(M + Cat)^+$ complexes were prepared by mixing small amounts (μg) of the peptides with one of the FAB matrices, which had been previously saturated with an alkali iodide.

Most mass spectrometric experiments were performed by using a VG 70-S, foward-geometry (EB, in which E = ESA and B = magnet) mass spectrometer (at Emory). The VG 70-S is equipped with an Ion Tech saddle-field FAB gun and a commercial FAB ion source. Precursor ions were produced by bombarding the sample with 7-keV Ar atoms at an atom gun current of 2 mA and were accelerated to 8-keV translational energy. Product ions that were formed metastably or by collision with He (analyzer pressure of 1×10^{-6} Torr; ~50% beam reduction) in the first field-free region between the ion source and the ESA were observed by using B/E scans. Experiments were performed at a product ion resolution of approximately 1000 (10% valley), and magnet calibration was performed by using a mixture of LiI, NaI, RbI, and CsI in H_2O. All spectra were acquired by using VG software, and metastable ion and CID spectra are the result of averaging between 10 and 20 scans. Background spectra were acquired for all experiments in order to eliminate artifact product ions that might arise from chemical noise.[4d]

The MS-MS and MS-MS-MS (MS^3) experiments involved using a JEOL HX110/HX110, tandem, four-sector (EB_1-EB_2) mass spectrometer (at the Structural Biochemistry Center, University of Maryland Baltimore County, or UMBC). Precursor ions were produced by using a JEOL FAB gun and 6-keV Xe atoms. Here, all CID spectra were acquired at 10-kV accelerating voltage by using He at 70% beam reduction. The MS-MS experiments were performed by using EB_1 to energy and mass select the $(M + Cat)^+$ complexes, which were then collided with He in a collision cell in the third field-free region. A linked scan of EB_2 was used to obtain spectra of the first-generation product ions. The MS^3 experiments were performed by colliding the $(M + Cat)^+$ complexes with He in the first field-free region between the FAB ion source and EB_1 and then using EB_1 to energy and mass select first-generation product ions. The selected first-generation ("intermediate") product ions were then collided with He in the third field-free region between EB_1 and EB_2. A linked scan of EB_2 was then used to obtain a spectrum of the second-generation product ions. Resolution was approximately 1000 for both EB_1 and EB_2, and MS^3 spectra are the result of a averaging between 2 and 10 scans.

Acknowledgment. The Emory University Research Fund and the donors of the Petroleum Research Fund, administered by the American Chemical Society, provided partial support for this research. Recognition is made to the NIH for the use of the VG 70-S, a shared instrument, and to the NSF for the use of the JEOL HX110/HX110 at the Structural Biochemistry Center at the University of Maryland Baltimore County, an NSF supported Biological Instrumentation Center. A preliminary report of these results was presented at the 38th ASMS Conference on Mass Spectrometry and Allied Topics, June 1990, Tucson, Arizona.

Registry No. RVYVHPF, 16376-83-3; YGGFLK, 83404-43-7; HLGLAR, 66157-45-7; RYLPT, 57966-42-4; VHLTP, 93913-38-3; YPFPG, 72122-63-5; YGGFM, 58569-55-4; FFFFF, 65757-10-0; BOC-YAG[*N*-Me]FG-01, 126616-16-8; YGGFL, 58822-25-6; YGGFL-NH_2, 60117-24-0; FLEEI, 62733-72-6; FLEEL, 69729-06-2; ALAL, 84676-48-2; ALAL-OMe, 131131-84-5; FFFF, 2667-02-9; GPRP, 67869-62-9; Ac-GPRP-OMe, 132884-57-2; GPGG, 13054-03-0; VAAF, 21957-32-4; VAAF-OMe, 131131-85-6; AGFL, 119530-65-3; GGFL, 60254-83-3; AGFM, 126616-17-9; GGFM, 61370-88-5; GGFM-NH_2, 84969-59-5; Ac-GGFM-OMe, 132884-58-3; ALG, 60030-20-8; GLY, 4306-24-5; MLF, 59881-08-2; GLF, 103213-38-3; GGV, 20274-89-9; GGV-OMe, 66328-83-4; FFF, 2578-81-6; IPI, 90614-48-5; PhCO-GGG, 31384-90-4; PhCO-GHL, 31373-65-6; 4-HOC_6H_4CO-GHL, 77697-23-5; AAA-OMe, 30802-27-8; AL, 3303-34-2; IN, 59652-59-4; LG, 686-50-0; LG-OMe, 27560-15-2; FF, 2577-40-4; LL, 3303-31-9; LL-OMe, 13022-42-9; GH, 2489-13-6; PhCO-GK, 740-63-6; PhCO-GF, 744-59-2; GL-NH_2, 17331-92-9; PhCO-[*N*-Me]G[*N*-Me]F-OMe, 132884-59-4; Ac-LG, 4033-42-5; Ac-GGV, 97530-33-1; Ac-YGGFL-NH_2, 132910-39-5; Ac-GGFM-NH_2, 132884-60-7; LiI, 10377-51-2; NaI, 7681-82-5; KI, 7681-11-0; RbI, 7790-29-6; CsI, 7789-17-5.

Migratory Insertion of Ethylene into Iron-Hydrogen Bonds and β-Hydride Elimination of Ethyl Groups on H-Covered Fe(100)

M. L. Burke[†] and R. J. Madix*[,‡]

Contribution from the Department of Chemistry and the Department of Chemistry and Chemical Engineering, Stanford University, Stanford, California 94305. *Received October 22, 1990. Revised Manuscript Received January 14, 1991*

Abstract: Ethylene has been found to adsorb reversibly at 110 K without dissociation on Fe(100) presaturated with hydrogen. No ethane is formed following adsorption of ethylene, nor does any ethylene decompose on this surface. Desorption of ethylene at 160 K competes with the formation of adsorbed ethyl groups. Ethyl groups decompose by β-hydride elimination with an activation barrier of 12.2 ± 0.6 kcal/mol and a preexponential factor of $10^{13.4\pm0.6}$ s^{-1}, exhibiting a primary kinetic isotope effect, k_H/k_D, at 219 K of 4.9 ± 0.5. The reversible reaction of adsorbed ethylene and adsorbed deuterium to form ethyl groups leads to the incorporation of up to four D atoms in the ethylene evolved during temperature-programmed reaction. The activation energies determined here indicate that barriers to formation and β-hydride elimination of adsorbed ethyl groups agree with those observed for transition-metal complexes only after the energetics of structural rearrangements in the complex are removed.

1. Introduction

Over the last 10 years there has been considerable interest in the "cluster-surface analogy".[1-3] In order to contribute to the general understanding of transition-metal chemistry in all of its regimes, we have undertaken surface studies of one of the most fundamental and well-studied homogeneous catalytic reactions, olefin hydrogenation. In the present study we have directed our efforts toward the elucidation of the fundamental kinetic and mechanistic aspects of ethylene hydrogenation on an iron surface.

* Author to whom correspondence should be addressed.
† Department of Chemistry.
‡ Department of Chemistry and Chemical Engineering.

(1) Muetterties, E. L. *Bull. Soc. Chim. Belg.* **1975**, *84*, 959.
(2) Muetterties, E. L.; Rhodin, T. N.; Band, E.; Brucker, C. F.; Pretzer, W. R. *Chem. Rev.* **1979**, *79*, 91.
(3) Canning, J.; Madix, R. J. *J. Phys. Chem.* **1984**, *88*, 2437.

0002-7863/91/1513-3675$02.50/0

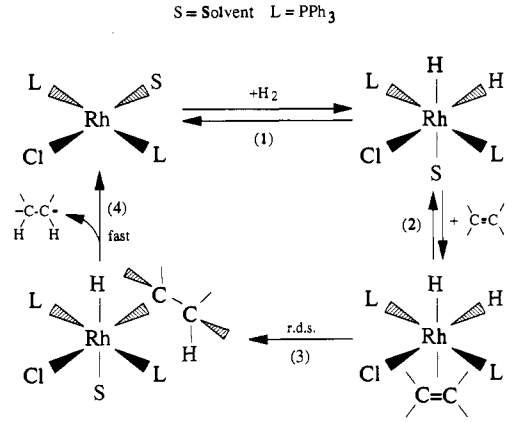

Figure 1. Schematic of the catalytic cycle of Wilkinson's hydrogenation catalyst.

Ethylene is a logical olefin to begin with due to its simplicity, and iron was chosen because (1) it is a first-row metal and thus a suitable place to begin a comparative study, (2)) there is a wealth of literature on iron chemistry in mononuclear complexes for a wide variety of reactions, and (3) it is one of the few metals which form small clusters stable enough to remain intact during homogeneous reactions, thus adding a possible dimension for comparative studies. We report here on the reversible binding of ethylene to the Fe(100) surface presaturated with adsorbed hydrogen atoms and the reversible formation of surface-bound ethyl groups.

The quintessential homogeneous hydrogenation catalyst is $RhCl(PPh_3)_3$, or Wilkinson's catalyst (Figure 1); the active form of the catalyst, $RhCl(PPh_3)_2$, is formed via the loss of a PPh_3 ligand. Several classes of elementary reactions exhibited by transition-metal complexes are present in the catalytic cycle (Figure 1):[4] $RhCl(PPh_3)_2$ facilitates oxidative addition of H_2 (1) followed by reversible coordination of the olefin (2), next follows the rate-determining migratory insertion of the olefin into the M–H bond (3), and finally the rapid reductive elimination of the alkyl hydride liberates the alkane (4). This catalyst is extraordinarily selective, and neither H–D exchange nor olefin isomerization via double bond migration compete to a measurable extent with alkane formation. Both features are attributed to the rapid elimination of alkane from the alkyl hydride, with negligible β-hydride elimination, the reverse step of the migratory insertion (step 3). But $RhCl(PPh_3)_3$ is quite atypical in its activity and selectivity. For instance the complexes $HRh(CO)(PPh_3)_3$, $IrCl(CO)(PPh_3)_2$, and $IrCl(PPh_3)_2$ are all active hydrogenation catalysts but each is also active in olefin isomerization;[5,6] these three complexes all catalyze the formation of 2-alkenes during the hydrogenation of 1-alkenes.

In the realm of homogeneous cluster reactivity there is a dearth of information on kinetics and mechanisms compared to that available for homogeneous complexes. One problem that occurs in characterizing the catalytic activity of a cluster is the propensity of clusters to break up into smaller fragments which often act as the actual catalysts. One of the few transition-metal clusters that remains intact during hydrogenation of olefins is $H_2Os_3(CO)_{10}$.[7,8] Other clusters that may retain their metal atom content during olefin hydrogenation are $H_4Ru_4(CO)_{12}$,[9,10] $[Ru_3O(O(CO)CH_3)_6]^+$,[11] and $Rh_6(CO)_{10}(PPh_3)_6$.[12] These clusters typically catalyze olefin hydrogenation and H–D exchange, and for the Ru_4 cluster the active catalyst is probably formed via the cleavage of a Ru–Ru bond in the tetrahedral cluster to yield a "butterfly" structure.[13]

Typically, studies of surface reactions of C_2H_4 have not been conducted with coadsorbed hydrogen, and the focus of the work has been the mode of decomposition of ethylene. An exhaustive discussion of the literature is not given here, but the literature relevant to this work will be discussed briefly. Some studies in the literature report that ethylene will *not* self-hydrogenate on many metal surfaces, including W(100),[14] Re(001) and Re(poly),[15] Ru(001),[16] Rh(100) and Rh(111),[17,18] Ir(111),[19] Ni(100),[20,21] Ni(111),[22-24] Ni(poly),[25] Pd(100),[26,27] Pd(110) and Pd(111),[27] and Pt(111).[28] In contrast, small amounts of ethane apparently have been reported to desorb from ethylene self-hydrogenation on the W(100), -(111), -(110), and -(112) faces[29] as well as on Pt(111).[30] Clearly there is not total agreement on this point. Typically, however, numerous modes of *decomposition* have been discovered, leading to the formation of (1) a vinyl intermediate on Ni(100)[31] and Pd(100),[26] (2) adsorbed acetylene on W(100),[32] Ni(111),[33] and Pt(100),[34] (3) acetylide on Ru(001)[16] and Rh(100),[35] (4) vinylidene on Pt(100)[34] as well as (5) ethylidyne on Ru(001),[16] Rh(100),[35] and the (111) faces of Pt,[36,37] Pd,[38] Rh,[39] Ir,[40] and Ni.[41]

Relatively few studies have addressed the effect of coadsorbed hydrogen on ethylene adsorption and reaction, and thus there is little basis for the comparison of hydrogenation on surfaces with that in complexes. C_2H_4 coadsorbed with deuterium on the (100), (111), (110), and (112) W surfaces yields ethane incorporating up to six deuterium atoms, and less than 1.5% of the ethylene initially adsorbed is converted.[29] In contrast, no ethane formation was observed in a separate study on W(100) when ethylene and hydrogen were coadsorbed,[14] yet the ethylene evolved from the deuterium-precovered surface contained up to four D atoms, and C–H bond activation is clearly implied. Decomposition is clearly affected by adsorbed hydrogen on Ru(001); the preadsorption of

(4) Halpern, J.; Okamoto, T.; Zakhariev, A. *J. Mol. Catal.* **1976**, *2*, 65.
(5) Collman, J. P.; Hegedus, L. S. *Principles and Applications of Organotransition Metal Chemistry*; University Science: Mill Valley, CA, 1980; Chapter 6.
(6) James, B. R. *Homogeneous Hydrogenation*; Wiley: New York, 1973.
(7) Bradley, J. S. In *Metal Clusters*; Moskovits, M., Ed.; Wiley: New York, 1986.
(8) Keister, J. B.; Shapley, J. R. *J. Am. Chem. Soc.* **1976**, *98*, 1056.
(9) Lausarot, P. M.; Vaglio, G. A.; Valle, M. *Inorg. Chim. Acta* **1977**, *25*, L107.
(10) Doi, Y.; Koshizuka, K.; Keii, T. *Inorg. Chem.* **1982**, *21*, 2732.
(11) Fouda, S. A.; Rempel, G. L. *Inorg. Chem.* **1979**, *18*, 1.
(12) Reinman, W.; Abboud, W.; Basset, J. M.; Mutin, R.; Rempel, G. L.; Smith, A. K. *J. Mol. Catal.* **1980**, *9*, 349.
(13) Rossetti, R.; Stanghellini, P. L. *Inorg. Chim. Acta* **1983**, *70*, 121.
(14) Pearlstein, K. A.; Friend, C. M. *J. Vac. Sci. Technol. A* **1984**, *2*, 1021.
(15) Ducros, R.; Housley, M.; Alnot, M.; Cassuto, A. *Surf. Sci.* **1978**, *71*, 433.
(16) Hills, M. M.; Parmeter, J. E.; Mullins, C. B.; Weinberg, W. H. *J. Am. Chem. Soc.* **1986**, *108*, 3554.
(17) Dubois, L. H.; Castner, D. G.; Somorjai, G. A. *J. Chem. Phys.* **1980**, *72*, 5234.
(18) Castner, D. G.; Sexton, B. A.; Somorjai, G. A. *Surf. Sci.* **1978**, *71*, 519.
(19) Nieuwenhuys, B. E.; Somorjai, G. A. *Surf. Sci.* **1978**, *72*, 8.
(20) Schoofs, G. R.; Benziger, J. B. *Langmuir* **1988**, *4*, 526.
(21) Zaera, F.; Hall, R. B. *Surf. Sci.* **1987**, *180*, 1.
(22) Klimesch; Henzler, M. *Surf. Sci.* **1979**, *90*, 57.
(23) Demuth, J. E. *Surf. Sci.* **1978**, *76*, L603.
(24) Bertolini, J. C.; Rousseau, J. *Surf. Sci.* **1979**, *83*, 531.
(25) Benninghoven, A.; Beckmann, P.; Greifendorf, D.; Schemmer, M. *Appl. Surf. Sci.* **1980**, *6*, 288.
(26) Stuve, E. M.; Madix, R. J. *J. Phys. Chem.* **1985**, *89*, 105.
(27) Gentle, T. M.; Muetterties, E. L. *J. Phys. Chem.* **1983**, *87*, 2469.
(28) Berlowitz, P.; Megiris, C.; Butt, J. B.; Kung, H. H. *Langmuir* **1985**, *1*, 206.
(29) Cartier, P. G.; Rye, R. R. *J. Catal.* **1974**, *32*, 88.
(30) Godbey, D.; Zaera, F.; Yeates, R.; Somorjai, G. A. *Surf. Sci.* **1986**, *167*, 150.
(31) Zhu, X.-Y.; Castro, M. E.; Akhter, S.; White, J. M. *Surf. Sci.* **1988**, *207*, 1.
(32) Hamilton, J. C.; Swanson, N.; Waclawski, B. H.; Celotta, R. J. *J. Chem. Phys.* **1981**, *74*, 4156.
(33) Lehwald, S.; Ibach, H. *Surf. Sci.* **1979**, *89*, 425.
(34) Hatzikos, G. H.; Masel, R. I. *Surf. Sci.* **1987**, *185*, 479.
(35) Slavin, A. J.; Bent, B. E.; Kao, C.-T.; Somorjai, G. A. *Surf. Sci.* **1988**, *206*, 124.
(36) Steininger, H.; Ibach, H.; Lewald, S. *Surf. Sci.* **1982**, *117*, 685.
(37) Kesmodel, L. L.; Dubois, L. H.; Somorjai, G. A. *Chem. Phys. Lett.* **1978**, *56*, 267.
(38) Gates, J. A.; Kesmodel, L. L. *Surf. Sci.* **1983**, *124*, 68.
(39) Koel, B. E.; Bent, B. E.; Somorjai, G. A. *Surf. Sci.* **1984**, *146*, 211.
(40) Marinova, Ts. S.; Kostov, K. L. *Surf. Sci.* **1987**, *181*, 573.
(41) Zhu, X.-Y.; White, J. M. *Catal. Lett.* **1988**, *1*, 247.

hydrogen greatly reduces the amount of *decomposition* of ethylene.[42] Extrapolation of these results from the maximum coverage studied of 0.85 monolayer of hydrogen leads to the conclusion that no ethylene decomposition would occur at a hydrogen precoverage of 1 monolayer (ML). Only trace amounts of ethane were evolved in these experiments with Ru(001), and no ethyl intermediates were observed by electron energy loss vibrational spectroscopy (EELS).

On the (100), (110), and (111) faces of Pd[27,43] as well as on Pt(111)[28,30] hydrogenation readily occurs, yet attempts to hydrogenate ethylene on Ni(100) have been unsuccessful.[20] Only on Pt(111) have kinetic studies been performed;[30] in this case reaction between adsorbed hydrogen and ethyl groups was proposed as the rate-determining step to form ethane. The kinetics of $C_2H_{5(a)}$ formation and β-hydride elimination could not be determined separately, and the measured rates were fit by varying ΔH and ΔS for the preequilibrium, $H_{(a)} + C_2H_{4(a)} \leftrightarrow C_2H_{5(a)}$. The kinetic parameters obtained for reductive elimination of ethane were 6 kcal/mol for the activation energy and $10^{-2.8}$ cm^2/s for the preexponential factor. To the best of our knowledge there is no previous work in which ethyl groups have been isolated in the hydrogenation of ethylene on metal surfaces.

There are relatively few studies of ethylene reactions on iron single-crystal surfaces. Ethylene does not self-hydrogenate on the Fe(100)[44] or the Fe(111)[45] face. On all clean Fe surfaces ethylene readily decomposes. Vibrational spectra have shown that C_2H_4 adsorbed near 100 K is strongly rehybridized to sp^3.[45,46] Decomposition on Fe(111) proceeds directly to adsorbed carbon and hydrogen at 250 K,[45] and on Fe(110) on adsorbed acetylene intermediate is formed at 300 K which further decomposes above 400 K.[46] Vibrational studies have not been conducted for Fe(100), but ultraviolet photoelectron spectroscopy (UPS) indicates that the C–C bond may be cleaved upon adsorption at 98 K.[47,48] We report here the first studies of the reactive interactions of coadsorbed ethylene and hydrogen on iron single-crystal surfaces. These studies show strong evidence for the reversible formation of surface-bound ethyl groups.

2. Experimental Section

All experiments were performed in a stainless steel ultra-high-vacuum (UHV) chamber with a base pressure of 1×10^{-10} Torr. Reactions were monitored with temperature-programmed desorption/reaction (TPD/TPRS) utilizing a quadrupole mass spectrometer (UTI 100C) with a collimating orifice approximately 0.8 cm in diameter. A chromel–alumel thermocouple was spotwelded to the Fe(100) sample, and the mass spectrometer and thermocouple were interfaced to a computer. The mass spectrometer signal was multiplexed so up to eight masses could be monitored in a single experiment. The surface was cooled to temperatures as low as 110 K with liquid nitrogen. Separate capillary arrays were used to dose ethylene and hydrogen. Surface composition was determined by Auger electron spectroscopy (AES), and long-range ordering of adsorbates was monitored by low-energy electron diffraction (LEED).

Details of the preparation and initial cleaning of the Fe(100) crystal are given elsewhere.[49] Routine cleaning was achieved by Ar ion bombardment with a sample temperature of 700 K. This temperature was sufficiently high to allow diffusion of impurities from the bulk, but low enough to cause preferential segregation of carbon at the surface, so it could be sputtered away more effectively. After each bombardment the crystal was annealed at 1020 K for 30 s. This anneal resulted in a sharp p(1×1) LEED pattern. Bulk impurity levels were low enough that impurity segregation to the surface did not occur at the temperatures reached during TPRS. Surface cleanliness was determined by AES; absolute coverages of carbon, oxygen, and sulfur were calibrated in accordance with LEED patterns at known coverages. Carbided and sulfided Fe(100) each display a c(2×2) pattern at the adatom saturation coverages of 0.5 ML, where 1 ML equals the Fe(100) surface atom density of 1.22×10^{15} atom/cm^2. A c(2×2) pattern is also formed by saturation of the CO dissociative state, resulting in surface coverages of 0.25 ML each for carbon and oxygen.

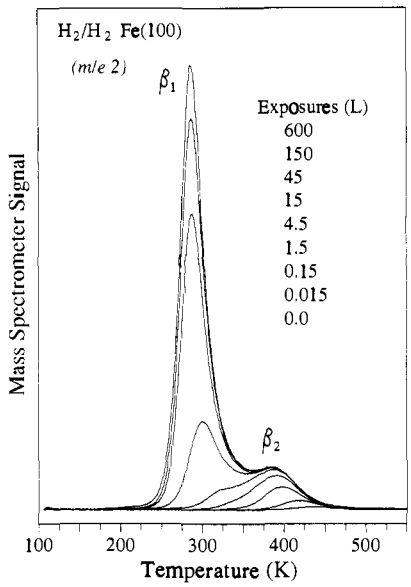

Figure 2. Hydrogen thermal desorption from Fe(100). Heating rates are approximately 10 deg K/s.

TPD/TPRS experiments were performed by dosing gases while the Fe sample was held at 110 K and by desorbing species through the collimator directly into the mass spectrometer. Absolute exposures of hydrogen were calibrated via a combination of background and direct doses as described previously.[49] Ethylene has both a high sticking probability and a large enhancement factor for direct dosing, the sum of which results in a large uncertainty in experimental values of the exposure. Absolute ethylene exposures therefore were not determined.

Absolute yields of ethylene TPRS states were estimated by applying a hydrogen and deuterium balance to the products of the H–D exchange reaction of C_2H_4 on the D-saturated Fe(100) surfaces (section 3.3). The saturation coverages of hydrogen[49] and deuterium[50] on Fe(100) have been previously determined to be 1.0 ML. TPRS of ethylene on the hydrogen-saturated surface yields only gas-phase hydrogen and ethylene with no ethylene decomposition on the surface (section 3.2); the number of H adatoms deposited by C_2H_4 adsorbed on D-saturated Fe(100) must therefore equal the number of D atoms incorporated into the desorbing ethylene products. TPRS traces for the parent ions of ethylene-d_n were deconvoluted to account for fragmentation of ethylene-d_m where $m > n$. The surface coverage of H adatoms (corrected for the 4% H adatom impurity found when the Fe(100) surface is exposed to D_2 saturation) was then equated to the D atom yield in ethylene products. By using the experimental relative TPRS areas, the equality was solved for the absolute yield (in ML) of a single ethylene isotope. The ratio of the yield to TPRS area was then used to convert other ethylene TPRS state areas to surface coverages.

Literature values for the fragmentation patterns of deuterated ethylenes[51] were used to deconvolute TPRS traces. The tabulated pattern for C_2H_4 agrees well with the cracking pattern determined with our mass spectrometer; thus the tabulated patterns for deuterated ethylenes should be applicable to the analysis of our experimental data. Conservative estimates of errors introduced by deconvolution were used in the derivatiion of our error limits of approximately 20% in stated ethylene coverages.[52] Since our collimated mass spectrometer detects products directly as they desorb, in a line-of-sight configuration, and since signals reflect gas-phase molecular densities and not fluxes,[53] a $T_S^{1/2}$ correction was made for the desorption temperatures of ethylene TPRS states. The

(42) Hills, M. M.; Parmeter, J. E.; Weinberg, W. H. *J. Am. Chem. Soc.* **1986**, *108*, 7215.
(43) Gentle, T. M.; Grassian, V. H.; Klarup, D. G.; Muetterties, E. L. *J. Am. Chem. Soc.* **1983**, *105*, 6766.
(44) Benziger, J. B.; Madix, R. J. *J. Catal.* **1980**, *65*, 49.
(45) Seip, U.; Tsai, M. C.; Kueppers, J.; Ertl, G. *Surf. Sci.* **1984**, *147*, 65.
(46) Erly, W.; Baro, A. M.; Ibach, H. *Surf. Sci.* **1982**, *120*, 273.
(47) Brucker, C.; Rhodin, T. *J. Catal.* **1977**, *47*, 214.
(48) Rhodin, T. N.; Brucker, C. F.; Anderson, A. B. *J. Phys. Chem.* **1978**, *82*, 894.
(49) Burke, M. L.; Madix, R. J. *Surf. Sci.* In press.
(50) Burke, M. L.; Madix, R. J. Unpublished results.
(51) Cornu, A.; Massot, R. *Compilation of Mass Spectral Data*, 2nd ed.; Heyden: New York, 1975; Vol. 1.
(52) Our error limits for ethylene coverages include uncertainties of (1) 25% in the relative TPRS areas of the deuterated ethylene products requiring deconvolution, (2) 5% in the relative TPRS areas of deuterated ethylenes requiring deconvolution, (3) 10% in the saturation coverage of H(D), (4) 10% in the H adatom yield following isotope exchange, and (5) 10% in the reproducibility of ethylene TPRS areas between experiments.
(53) Brown, L. S.; Sibener, S. J. *J. Chem. Phys.* **1989**, *90*, 2807.

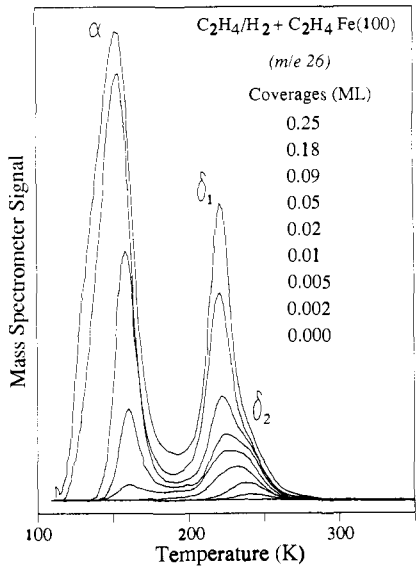

Figure 3. Temperature-programmed reaction spectra of ethylene from Fe(100)–H as a function of ethylene coverage. Heating rates are approximately 10 deg K/s.

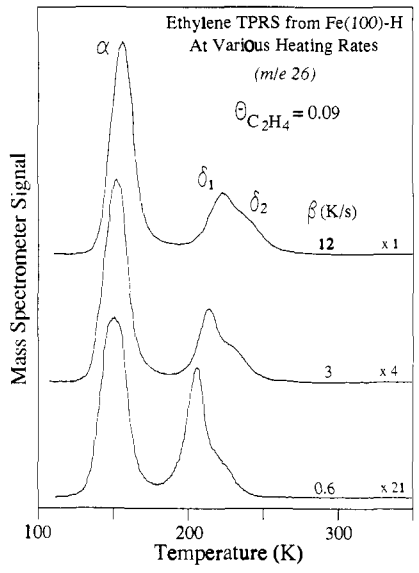

Figure 4. Temperature-programmed reaction spectra following adsorption of 0.09 ML of ethylene on Fe(100)–H for heating rates of 0.6, 3, and 12 deg K/s. Curves are normalized with respect to heating rate to give the same total area when plotted as rate versus temperature.

$T^{1/2}$ correction appears to be justified, based on the agreement between our calibrated CO coverages found by using this method with literature values for CO coverages determined via XPS.[49]

3. Results

3.1. Hydrogen TPD. Thermal desorption of hydrogen from Fe(100) has been described previously,[49] but there are several features germane to this work which we summarize here. Two H_2 desorption states attributed to hydrogen (H) adatom recombination fill sequentially as hydrogen exposure increases (Figure 2). The higher temperature (β_2) state displays apparent second-order kinetics; the peak temperature shifts down as coverage increases, and the peak is nearly symmetric about the maximum. At saturation coverage the β_2 state has a peak temperature, T_p, of 390 K and an absolute coverage of 1/8 ML. In contrast, the β_1 state displays pseudo-first-order kinetics; its peak temperature is constant with respect to initial coverage. Similar pseudo-first-order desorption of H_2 from W(100) has been ascribed to adatom–adatom repulsion at high coverages.[54] At saturation the peak temperature of β_1–H_2 is 290 K and the *total* surface hydrogen coverage is 1 ML.

Kinetic analysis of the β_1 state was performed by heating rate variation[55] with a resulting activation energy, E, of 16.8 ± 0.6 kcal/mol at Θ_H = 0.66, which is the H coverage at the peak desorption rate. The apparent first-order preexponential, A, is $10^{12.6\pm0.4}$ s^{-1}. Kinetic parameters for the β_2 state were estimated from T_p and the peak width at one-half of the maximum rate, $\Delta T_{1/2}$, by using the method of Chan et al.[56] The β_2 state is not perfectly second order, in that kinetic parameters extracted varied with the initial H coverage. In the limit of low Θ_H the values determined for E and A for the β_2 hydrogen state were 23.2 kcal and $10^{-1.5}$ cm^2/s, respectively.

A lower limit to the strength of the Fe–H bond was estimated from the kinetic parameters of the more weakly bound or β_1 state. An upper limit to the activation barrier to adsorption of H_2 was estimated from sticking probabilities to be 2 kcal/mol.[49] Including the gas-phase H–H bond energy of 104.2 kcal/mol[57] leads to an Fe–H bond strength of 59.5 kcal/mol.

3.2. Ethylene TPRS on Fe(100)–H. Ethylene adsorbed on the hydrogen-saturated Fe(100) surface (hereafter referred to as Fe(100)–H) evolves gas-phase C_2H_4 in three TPRS states: α, δ_1, and δ_2 (Figure 3). The small state at 235 K (δ_2) is present for all initial coverages of ethylene and saturates at about 0.01 ML; due to its low saturation coverage the δ_2-C_2H_4 state is attributed to defects. The stability of the adsorbed intermediate at defect sites is apparently greater than that for other sites, leading to a higher evolution temperature than that of the δ_1 state. Increasing the C_2H_4 coverage above 0.01 ML results in the simultaneous development of the α and δ_1 states at 160 and 220 K, respectively. These states grow in together with apparent first-order kinetics; i.e. the peak temperatures remain constant as the initial coverage is initially increased. As saturation is approached, however, the α state broadens, and its peak temperature shifts downward to 150 K. Repulsive interactions in the C_2H_4 adlayer are probably responsible for this effect at high ethylene coverages. For comparison, we have noted this to be a general characteristic of alkene desorption from weakly bound states on Ag.[58,59]

Hydrogen and ethylene were the only gas-phase species evolving during TPRS, with the exception of *trace* amounts of ethane; C_3 and C_4 hydrocarbons were monitored, but none were detected. Furthermore, no decomposition of C_2H_4 occurred on the hydrogen-presaturated surface; there was no increase in the hydrogen TPRS above that expected from the presaturation coverage of hydrogen on Fe(100), and no increase in surface carbon levels in AES spectra recorded after TPRS was detected. H_2 thermal desorption was not perturbed by ethylene postadsorption, because nearly all of the ethylene has desorbed prior to 250 K, the temperature at which hydrogen desorption from the clean surface becomes significant. The saturation coverage of C_2H_4 on Fe(100)–H is estimated to be 0.25 ± 0.05 ML (sections 2 and 3.3). The relative amounts of ethylene evolved via the α and δ_1 states at a fixed total coverage of ethylene were very sensitive to the heating rate used, reflecting a coupling of the kinetic processes giving rise to these two states (Figure 4). For a constant initial coverage of 0.09 ML of C_2H_4 on Fe(100)–H, the δ_2 state appears to maintain a constant population, whereas there is a shift in population from the δ_1 to the α state as the heating rate increases. This result suggests that α desorption and δ_1 state formation are competitive activated processes.

The activation energy for evolution via the α state is clearly higher than that for δ_1 formation. On the basis of the kinetics of branched reactions,[60] the branching ratio, B, of two first-order-reaction channels is given by

(54) King, D. A. *Surf. Sci.* **1975**, *47*, 384.
(55) Falconer, J. L.; Madix, R. J. *Surf. Sci.* **1975**, *48*, 393.
(56) Chan, C.-M.; Aris, R.; Weinberg, W. H. *Appl. Surf. Sci.* **1978**, *1*, 360.
(57) Benson, S. W. *Thermochemical Kinetics*, 2nd ed.; Wiley: New York, 1976.
(58) Capote, A. J.; Madix, R. J. To be published.
(59) Roberts, J. T.; Madix, R. J. To be published.
(60) Hall, R. B. *J. Phys. Chem.* **1987**, *91*, 1007.

$$B = \frac{r_1}{r_2} = \frac{A_1}{A_2} e^{-(E_1-E_2)/RT} \quad (1)$$

and in a TPRS experiment

$$T = T_0 + \beta t \quad (2)$$

Here r is the reaction rate, R is the gas constant, T_0 is the initial temperature, β is the heating rate, and t is time. It follows that

$$\frac{dB}{d\beta} = B\frac{(T - T_0)}{\beta}\frac{(E_1 - E_2)}{RT^2} \quad (3)$$

All of the grouped terms on the right-hand side of eq 3 are positive except for $(E_1 - E_2)$, which may be positive or negative. It thus follows that

$$dB/d\beta > 0 \quad \text{for } E_1 > E_2$$

or

$$dB/d\beta < 0 \quad \text{for } E_1 < E_2 \quad (4)$$

Increasing β thus shifts the branching ratio, B, toward the reaction with the higher activation energy at the expense of the lower barrier reaction. The identification of the reaction branches leading to α-state evolution and δ_1-state formation and the evaluation of the rate constants is given below (section 3.5). First, however, we represent the results for H–D exchange and kinetic isotope effects.

3.3. H–D Exchange of C_2H_4 on Fe(100)–D. TPRS performed subsequent to C_2H_4 adsorption onto deuterium-presaturated Fe(100) shows that the α state does not undergo H–D exchange, while the δ states incorporate from 1 to 4 D atoms (Figure 5). Tabulated mass spectral cracking patterns for deuterated ethylenes[51] were used to correct each ethylene-d_n trace for fragmentation of ethylene products with higher deuterium content. After the correction there is no evidence for the evolution of any ethylene-d_0 in the δ states. Facile H–D exchange in the δ states with no exchange in the α state indicates that the α state arises from desorption of ethylene which has not undergone H atom addition or C–H bond activation, whereas the δ states evolve from a surface intermediate in which C–H bonds have been broken and formed. The α state is clearly due to molecularly adsorbed ethylene. Possible intermediates leading to the δ state are ethyl groups (C_2H_5), vinyl, or ethylidyne (C_2H_3). No deuterated ethylene is observed in the α state, even in the trailing edge. The results suggest that H–D exchange occurs at the temperatures of evolution of the δ states through the reversible formation of an adsorbed intermediate, written here as an ethyl group.

$$C_2H_{5(a)} \underset{-1}{\overset{1}{\rightleftharpoons}} C_2H_{4(a)} + H_{(a)} \xrightarrow{2} C_2H_{4(g)} + H_{(a)} \quad (5)$$

In this case, chemisorbed ethylene formed from β-hydride elimination of the ethyl intermediate may either convert to an ethyl group (−1), allowing another D to be incorporated into the molecule, or desorb into the gas phase (2). Similar schemes would result in multiple H–D exchange for vinyl or ethylidyne. At the temperature in the temperature-programmed reaction at which this exchange occurs both desorption and conversioin of molecularly adsorbed ethylene are rapid.

The relative amounts of the deuterated ethylenes evolved may be understood in a qualitative sense on the basis of the kinetics of formation and reaction of the α, δ_1, and δ_2 states. First of all, the C_2D_4 product can be almost completely attributed to the δ_2 ethylene state. Only about 0.016 ML of C_2D_4 is evolved, which is only slightly greater than the δ_2 state saturation population of 0.012 ML, and the peak is shifted abruptly upward in temperature relative to the d_1–d_3 products. This effect reflects the higher desorption temperature of the δ_2 state relative to that of δ_1 for C_2H_4 on Fe(100)–H. However, the role of kinetic isotope effects and the requirement that the $\delta \leftrightarrow \alpha$ state transformation occurs repeatedly before ethylene-d_4 evolves complicates the assignment of this isotope entirely to the δ_2 state. Because of these complexities the multiple H–D exchange kinetics were not explored in greater detail.

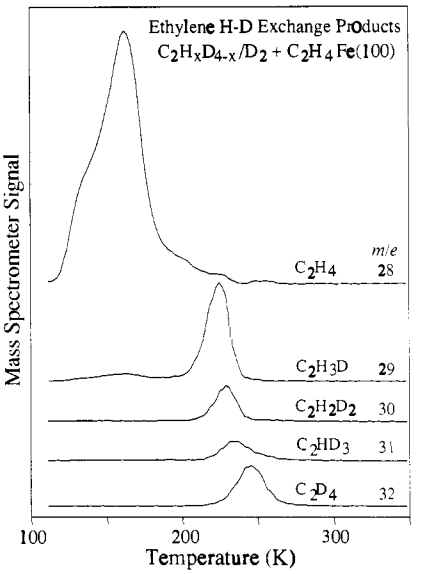

Figure 5. Temperature-programmed reaction spectra of deuterated ethylene products evolved from C_2H_4 on Fe(100)–D. Traces for each ethylene-d_n product have been corrected for mass spectral fragmentation of ethylene-d_m, where $m > n$. The heating rate is approximately 10 deg K/s.

Table I. Experimental and Statistical Isotope Distribution for H–D Exchange of C_2H_4 on Fe(100)–D

		expt values		statistical mixing ratios[a]	
product	isotope	Θ, ML	ratios	intraspecies	interspecies
hydrogen	H_2	0.04	1.0	1.0	1.0
	HD	0.29	7.6	8.8	7.3
	D_2	0.67	17.0	19.4	13.3
ethylene	d_0	0.000	0.0	0.2	0.1
	d_1	0.032	1.0	1.0	1.0
	d_2	0.011	0.35	1.7	5.5
	d_3	0.010	0.29	1.3	13.3
	d_4	0.016	0.50	0.4	12.2

[a] Intraspecies mixing ratios for a given product are calculated by using the experimental H/D ratio found for that product only. Interspecies mixing values are calculated with the global H/D ratio.

The distribution of D in the d_1–d_4 products is nonstatistical (Table I) since both the d_1 and d_4 populations are greater than that of d_2 and d_3, and no ethylene-d_0 was detected. The H:D ratio in the H_2, HD, and D_2 which desorbs is 1:4.4 while the H:D ratio is 1:1.15 in the ethylene evolved in the δ states, again demonstrating that the distribution of D is not statistical. The absence of ethylene-d_0 in the δ states is consistent with preferential breaking of C–H bonds in the intermediate and supports our conclusion that C–H bond cleavage is the rate-limiting step for δ ethylene (section 3.4). The nonstatistical distribution of deuterium in the ethylene-d_1 and -d_2 further indicates that the rate of desorption of chemisorbed ethylene is greater than the rate of reformation of the δ_1 intermediate in the temperature range where δ ethylene is evolved, thus only a limited number of H–D exchanges occur. The peak temperature of ethylene-d_1 matches that of the δ_1 state for C_2H_4 on Fe(100)–H. The slight upward shift in peak temperatures of the d_2 and d_3 peaks reflects the complex kinetics involved in the multiple exchange reactions mentioned above, coupled with kinetic isotope effects. Some ethylene-d_4 may be formed in the δ_1 state, but the amount is minor compared to that in the δ_2 state, given the sharp drop in population between d_1 and d_2 (Table I). Indeed, the high-temperature tail of ethylene-d_3 suggests a contribution from the δ_2 state. The falloff from d_2 to d_3 in the δ_1 state, therefore, is probably sharper than the total populations indicate.

3.4. Kinetic Isotope Effects in the Evolution of δ_1 Ethylene. Our kinetic isotope effect studies also indicate that β-hydride elimination of C_2H_4 from surface ethyl groups is responsible for the δ_1 state. The kinetic isotope effect for the evolution of δ_1-C_2D_4

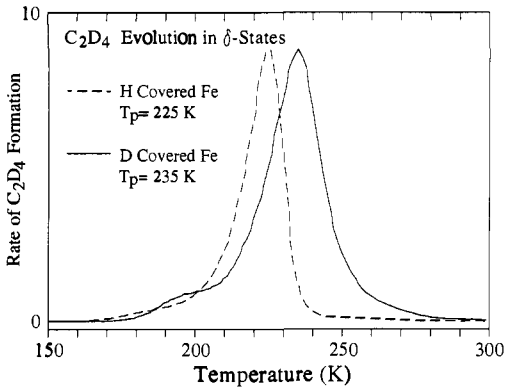

Figure 6. Evolution of C_2D_4 from C_2D_4 adsorbed on Fe(100)–D (solid line) and from C_2D_4 on Fe(100)–H (dashed line). The sample was annealed to 170 K at 0.5 K/s after adsorbing C_2D_4 and then cooled to approximately 130 K before the TPRS. The heating rates were 14 deg K/s.

following the adsorption of C_2D_4 on Fe(100)–H and Fe(100)–D was determined. If the intermediate were the ethyl group, $CD_2CHD_{2(a)}$ would be formed while $C_2D_{5(a)}$ would result on Fe(100)–D. The reaction responsible for C_2D_4 evolution in the δ_1 state would then be β-hydride(D) elimination. A primary kinetic isotope effect is expected in this case, since C–H bond cleavage would occur to give C_2D_4 on Fe(100)–H as compared to C–D cleavage on Fe(100)–D.[61] Conversely, if a surface-bound vinyl intermediate were responsible for the δ_1 state, the reaction yielding C_2D_4 on *both* the H- and D covered surfaces would be the addition of a D adatom to $C_2D_{3(a)}$, and no kinetic isotope effect would be observed. Other intermediates involving the addition of D, e.g. vinylidene (=C=CD_2), would show the same behavior as vinyl groups. In the case of ethylidyne (≡CCD_3 or ≡$CCHD_2$) a possible rate-determining step could be H(D) transfer from the β-carbon to either the surface or to the α-carbon, resulting in a large primary kinetic isotope effect. However, D adatom addition to the α carbon of ethylidyne could also be a rate-determining step, and in this case no kinetic isotope effect would result in our experiments. Implications of the kinetic isotope effect resulting from ethylidyne formation are thus ambiguous. However, involvement of this species is quite improbable, since it is highly thermally stable on all other surfaces. For example, decomposition occurs only above 330 K on Ni(111)[41] and Ru(001)[16] and above 450 K on Pt(111).[62] Ethylidyne also decomposes on these surfaces to give $H_{2(g)}$ and $C_{(a)}$ as the final products, not ethylene. Furthermore, we have found that the δ intermediate on Fe(100)–H may be hydrogenated to yield ethane in the presence of coadsorbed CO,[63] but it has been shown that ethylidyne is *not* the intermediate which leads to ethane formation on Pt(111),[30,64] or on supported Pd particles.[65] We are thus led to conclude that a normal primary kinetic isotope effect is indicative of the formation of ethyl groups on the surface.

The kinetic isotope effect observed in C_2D_4 evolution indeed suggests that an ethyl group is responsible for the δ_1 state of ethylene. Quantitative studies of the kinetic isotope effect for β-hydride elimination of adsorbed ethyl were performed by monitoring C_2D_4 evolution following C_2D_4 adsorption on the H- and D-covered Fe(100) surfaces and C_2H_4 evolution in the δ_1 state following C_2H_4 adsorption on Fe(100)–H, respectively. TPRS results (Figure 6) show that after adsorption of C_2D_4 on Fe(100)–D the δ_1 state shifts upward in temperature from about 230 K by 10 K relative to C_2D_4 adsorbed on Fe(100)–H.[66] By using

Table II. Kinetic Parameters for β-Hydride (D) Elimination of Ethyl Groups

reactant	H or D transfer	E, kcal/mol	log A, s^{-1}	k_H/k_D (219 K)
(a) C_2H_5	H	13.2 ± 0.6	13.4 ± 0.6	
(b) C_2HD_4	H	12.8 ± 0.6	12.7 ± 0.6	
(c) C_2D_5	D	15.0 ± 0.7	14.2 ± 0.7	14.2 ± 0.7
primary shift (b – a)		–0.4	–0.7	1.9 ± 0.2
secondary shift (c – b)	2.2	1.5	4.9 ± 0.5	
combined (c – a)	1.8	0.8	9.4 ± 1.1	

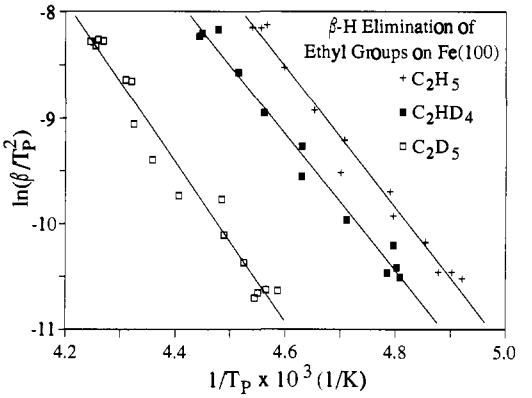

Figure 7. Heating rate variation kinetic plots for C_2H_4 from C_2H_4 on Fe(100)–H (+), C_2D_4 from C_2D_4 on Fe(100)–H (■), and C_2D_4 from C_2D_4 on Fe(100)–D (□). Solid lines are linear least-squares fits.

the method of heating rate variation,[55] kinetic parameters of 13.2 ± 0.6 kcal/mol and $10^{13.4\pm0.6}$ s^{-1} for E and A, respectively, were obtained for β-hydride elimination of C_2H_5 (Figure 7, Table II); values of E and A obtained for CD_2CHD_2 were 12.8 ± 0.6 kcal/mol and $10^{12.7\pm0.6}$ s^{-1}; the parameters for C_2D_5 were 15.0 ± 0.7 kcal/mol and $10^{14.2\pm0.7}$ s^{-1} (see Table II). Error limits on E and log A were obtained from the standard deviations of the slope and intercept, respectively, of the kinetics plots. For comparison, Lloyd et al. have observed recently that ethyl groups formed on Pt(111) by the photolysis of C_2H_5Cl are stable at 200 K, but decomposed by 230 K to yield adsorbed ethylene.[67]

The respective k_H/k_D values for the secondary, primary, and combined kinetic isotope effects evaluated at 219 K are 1.9 ± 0.2, 4.9 ± 0.5, and 9.4 ± 1.1. It can be seen directly from Figure 6 that the primary isotope effect for this first-order reaction must be greater than 2 at 220 K. Evaluation of k_H/k_D at 219 K requires no extrapolation because the peak temperatures for the three sets of isotope experiments intersect in a narrow region around this temperature. Error limits on k become prohibitively large upon extrapolation to 300 K, thus k_H/k_D cannot be accurately determined at that temperature. The error limits given for k_H/k_D are one standard deviation.[68] The propagation of errors in S and $Y(T_x)$ into k and k_H/k_D was treated as described elsewhere.[69]

(61) Note that a higher rate of C–H cleavage relative to C–D cleavage in CD_2CHD_2 implies that the majority species formed will be C_2D_4; thus interference from H–D exchange is minimized.
(62) Ogle, K. M.; Creighton, J. R.; Akhter, S.; White, J. M. *Surf. Sci.* **1986**, *169*, 246.
(63) Burke, M. L.; Madix, R. J. *J. Am. Chem. Soc.* Submitted.
(64) Zaera, F.; Somorjai, G. A. *J. Am. Chem. Soc.* **1984**, *106*, 2288.
(65) Beebe, T. P., Jr.; Yates, J. T., Jr. *J. Am. Chem. Soc.* **1986**, *108*, 663.

(66) The TPRS traces in Figure 6 were obtained by first annealing slowly to 170 K to desorb molecular ethylene and to maximize the δ_1 population, since high heating rates favor α desorption. In all cases ethylene was dosed to saturation on the Fe(100)–H(D) surface at 110 K. The sample was then annealed slowly at 0.5 ± 0.2 deg K/s to 170 K and recooled to 120 K before the TPRS. This slow annealing procedure estabished a fixed population of the δ_1 state prior to heating rate variations in order to examine the kinetic isotope effect of the δ_1 state. Peak temperatures were plotted as ln (β/T_p^2) vs $1/T_p$ to yield a line of slope $-E/R$ and an intercept of ln (AR/E).[55]
(67) Lloyd, K. G.; Campion, A.; White, J. M. *Catal. Lett.* **1989**, *2*, 105.
(68) To evaluate the error range, the rate constant was expressed as $k = E[\beta/(RT_p^2)]$, which is applicable for kinetic analysis via a heating rate variation for a first-order reaction.[55] The rate constant k is thus equal to $-S$ exp$[Y(T)]$, where the slope, S, is $-E/R$ and $Y(T) = \ln(\beta/T_p^2)$ at a given T_p on a plot of ln (β/T_p^2) versus $1/T_p$. Unlike A exp$(-E/RT)$, this form of k employs only values that can be accurately determined within the experimental data range. Error limits on k at a temperature T_x were evaluated by performing least-squares analysis of ln (β/T_p^2) versus $(1/T_p - 1/T_x)$; $Y(T_x)$ is thus the y intercept, and the uncertainty in $Y(T_x)$ is the standard deviation in the y intercept. Similarly, S and its standard deviation are equal to the least-squares values of the slope and its standard deviation.
(69) Skoog, D. A.; West, D. M. *Principles of Analytical Chemistry*, 2nd ed.; Saunders: Philadelphia, 1980; App. 1.

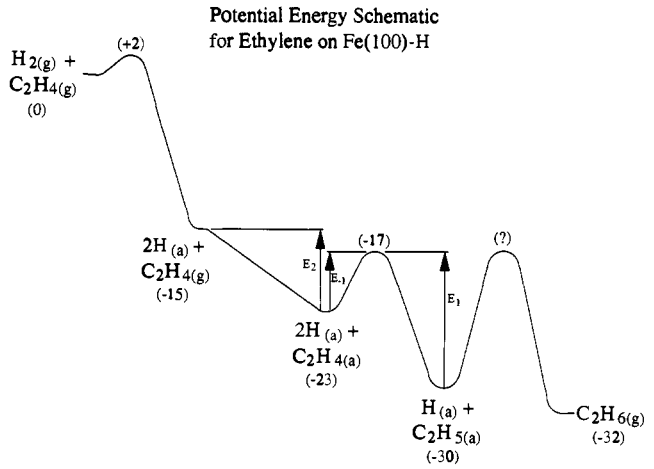

Figure 8. Potential energy schematic for the reactions of ethylene on Fe(100)–H. Numbers in parentheses give the potential energy of the system relative to $H_{2(g)}$, $C_2H_{4(g)}$, and the clean surface.

Kinetic isotope effects measured for the β-hydride elimination of Co[70] and Ir[71] mononuclear alkyl complexes suggest that those we observe on Fe(100) are large enough to arise from β-hydride elimination. For both complexes β-hydride elimination of the alkyl has been determined to be the rate-determining step for decomposition. Values of k_H/k_D at 300 K of 2.30 and 2.28 have been found upon perdeuteration of the alkyl β carbon for Co(ethyl)[70] and Ir(*n*-octyl) complexes, respectively.[71] Although extrapolation is dangerous, a rough estimate of the kinetic isotope effects at 219 K for the Co and Ir complexes is found by assuming that the preexponentials do not change upon deuteration, yielding an estimated primary kinetic isotope effect of 3.1 at 219 K. Our observed value of 4.9 thus is consistent with β-hydride elimination.

3.5. Kinetics of Ethyl Group Formation. The coupled kinetics of $C_2H_{4(a)}$ desorption and ethyl group formation are now considered. A schematic potential surface for the hydrogenation of ethylene on Fe(100)–H is shown in Figure 8. Potential minima are shown for both chemisorbed ethylene and the ethyl group. A third well due to a precursor for ethylene adsorption probably exists[72] but is not shown. The relative rate constants for ethyl group formation and ethylene desorption determine the relative magnitudes of ethylene evolved in the α and δ_1 states upon varying heating rate.

Computer simulations of the coupled reactions were performed assuming simple first-order kinetics for both C_2H_4 desorption and the migratory insertion to form C_2H_5.[73] The latter reaction is pseudo-first-order since the surface is saturated with hydrogen, and the ethyl groups formed probably block the site vacated by the H adatom involved in the migratory insertion reaction. No vacant H binding sites will develop during the reaction, and the local H coverages will stay fixed at 1 ML through the reaction. Experimental evidence for this is the lack of adsorption of additional hydrogen for 300-L H_2 exposures after annealing an ethylene-covered Fe(100)–H surface to 170 K to isolate ethyl groups. This result also suggests that no H vacancies are required during β-hydride elimination of C_2H_5, thus that reaction is first order in adsorbed alkyl and independent of Θ_H.

The rate constants were determined for a constant initial ethylene coverage of 0.09 ML on Fe(100)–H (see Figure 4). This coverage is high enough to yield a distinct δ_1 peak but low enough to avoid the kinetic complications of repulsive interactions in the C_2H_4 adlayer (Figure 3). The δ_2 state saturates at 0.01 ML before the α and δ_1 states grow in and thus has a constant population in the heating rate variations. This 0.01 ML was subtracted from the total δ state population since formation of δ_2 appears to be unactivated and independent of the two reaction steps being modeled here. Possible errors in the δ_1 population introduced by subtracting the δ_2 state should not significantly affect our results. To determine the four kinetic parameters four experimental quantities were employed, two of which were T_p and $\Delta T_{1/2}$ of the α desorption state. The remaining fitting constraints for the simulations were taken from a plot of the fraction of ethylene forming δ_1 ethyl groups, $\delta_1/(\alpha + \delta_1)$, as a function of the natural log of the heating rate, ln (β) (Figure 9). The data are well represented by a straight line fit via linear least-squares analysis. The slope and midpoint of this line were chosen as the final two experimental quantities needed to uniquely determine kinetic parameters with the computer simulations. Small variations in

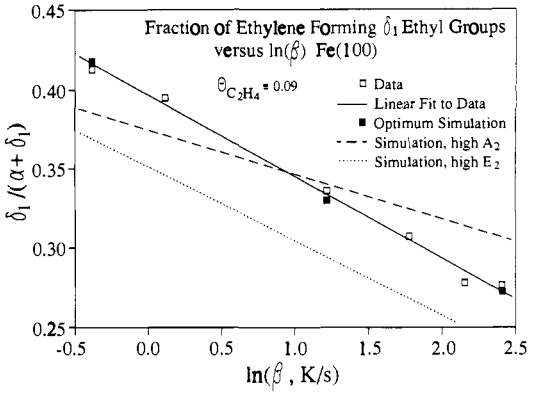

Figure 9. Fraction of $\alpha + \delta_1$ ethylene in the δ_1 state as a function of the natural log of the heating rate. Data points (□) and points generated from an optimized simulation of a branched reaction (■) are shown. The solid line is a linear least-squares fit to the data. The dashed line represents simulations with log (A_{-1}) 1 unit higher than optimum, with E_{-1} reoptimized. The dotted line was generated by using the optimal A_{-1} in the simulations, but with E_{-1} 0.05 kcal higher than optimum.

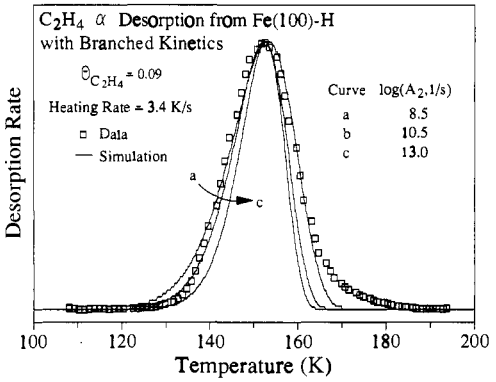

Figure 10. Temperature-programmed reaction data and simulations for the ethylene α state. The simulated curves are generated by using branched kinetics for α desorption and δ_1 formation. The preexponential for desorption was varied from its optimal value of $10^{8.5}$ to a normal value of 10^{13} s^{-1}.

Table III. Kinetic Parameters from Simulations of Ethylene Desorption (2) (A_2, E_2) Competing with Ethyl Formation (A_{-1}, E_{-1})

simulation	A_2, s^{-1}	E_2, kcal/mol	A_{-1}, s^{-1}	E_{-1}, kcal/mol	ΔE, kcal/mol
optical	$10^{8.5}$	6.3	$10^{6.0}$	4.8	1.5
A_2 fixed	$10^{9.5}$	6.9	$10^{6.8}$	5.3	1.6
A_2 fixed	$10^{10.5}$	7.6	$10^{7.6}$	5.8	1.8
A_2 fixed	$10^{13.0}$	9.3	$10^{9.6}$	7.2	2.1

(70) Ikariya, T.; Yamamoto, A. *J. Organomet. Chem.* **1976**, *120*, 257.
(71) Evans, J.; Schwartz, J.; Urquhart, P. W. *J. Organomet. Chem.* **1974**, *81*, C37.
(72) The ethylene sticking probability on Fe(100)–H remains near 1 over a considerable coverage range, indicting that ethylene may adsorb by a precursor mechanism.
(73) A fourth order Runge–Kutta routine was modified to simultaneously handle two reaction channels. A total of four adjustable parameters were used: A_{-1} and E_{-1} for ethyl formation along with A_2 and E_2 for ethylene desorption. For first-order kinetics the initial concentration, Θ_0, determines the absolute yield in each reaction channel, but the relative yields are invariant with respect to Θ_0.

the kinetic parameters used in the computer simulations result in large changes in calculated values of $\delta_1/(\alpha + \delta_1)$ versus ln (β) (see below, Figure 9). Conversely, variations in $\delta_1/(\alpha + \delta_1)$ values result in only small changes in kinetic parameters.[74]

With use of this procedure, optimal kinetic parameters were found to be $10^{8.5}$ s^{-1} (A_2) and 6.3 kcal/mol (E_2) for ethylene desorption; the values for C_2H_5 formation, A_{-1} and E_{-1}, were $10^{6.0}$ s^{-1} and 4.8 kcal/mol (Table III). These values give T_p and $\Delta T_{1/2}$ of 153 and 17.5 K for the α state for a 3.4 deg K/s heating rate and match the respective experimental values of 152.5 and 18 K well (Figure 10). Calculated values of $\delta_1/(\delta_1 + \alpha)$ also match experiment well, as shown by the filled squares in Figure 9.[75] The preexponential factors calculated in this fashion are lower than expected for simple first-order processes. Thus, in order to bracket the values of the kinetic parameters, additional simulations were performed with higher preexponentials for ethylene desorption. With A_2 fixed the other three kinetic parameters were determined by fitting T_p along with the slope and midpoint of the data for $\delta_1/(\alpha + \delta_1)$ versus ln (β). The fourth constraint, $\Delta T_{1/2}$, was excluded from these simulations. Values of A_2 of $10^{9.5}$, $10^{10.5}$, and $10^{13.0}$ s^{-1} were chosen, and the results for E_2, A_{-1}, and E_{-1} are listed in Table III. As expected, increasing A_2 led to increased E_2 values needed to obtain the experimental T_p for the α state, and the peak widths for the α state narrowed considerably upon increasing A_2 from $10^{8.5}$ to $10^{13.0}$ s^{-1} (Figure 10).

A reasonable range for each of the four kinetic parameters is bracketed by values found with the optimized simulations (resulting in low preexponentials) and those found with a preexponential factor for C_2H_4 desorption of 10^{13} s^{-1}. For C_2H_4 desorption the kinetic parameters are thus $10^{11\pm2}$ s^{-1} for A_2 and 8 ± 1.5 kcal/mol for E_2. For the migratory insertion of adsorbed C_2H_4 A_{-1} and E_{-1} are 108 ± 2 s^{-1} and 6 ± 1 kcal/mol, respectively. The *difference* between the activation energies for the two reaction branches is fairly insensitive to changes in the value of A_2 so the difference, $E_2 - E_{-1}$, can be estimted to be 1.8 ± 0.3 kcal/mol.

3.6. Interpretation of Kinetic Parameters for β-Hydride Elimination. Due to the coupling between the reactions of β-hydride elimination, migratory insertion, and ethylene desorption which all occur during the evolution of the δ_1 state, care must be exercised in the interpretation of the kinetic parameters for the δ_1 state. In particular the question arises as to whether E_1, the activation energy determined for δ_1 evolution, actually reflects the energy difference between the reactant well and the transition state for $C_2H_{4(a)}$ formation or whether the kinetics are influenced by having an adsorbed ethylene intermediate prior to evolution into the gas phase.

Kinetic equations accounting for the effects of molecular precursors on desorption also describe the β-hydride elimination of ethyl groups with the subsequent desorption of ethylene.[76,77] In the derivation of the overall rate equation for the evolution of gas-phase ethylene from surface ethyl groups on the H-saturated surface the kinetics were assumed to be first order in the hydrocarbon reactant and independent of the concentration of $H_{(a)}$ for each of the elementary steps of ethyl β-hydride elimination, ethyl formation, and ethylene desorption (section 3.5). The concentration of the chemisorbed C_2H_4 intermediate is assumed to be low during the β-hydride elimination reaction, so that the steady-state approximation may be invoked. As a result the rate of evolution of gas-phase ethylene, r, from $C_2H_{5(a)}$ β-hydride elimination is

$$r = \frac{k_1 k_2 c_{ethyl}}{k_2 + k_{-1}} \quad (6)$$

The rate constants apply to the steps illustrated in Figure 8, and c_{ethyl} is the surface concentration of ethyl groups. Equation 6 is slightly different from precursor equations[76] in that no $(1 - \Theta)$ dependence was included in the rate of ethyl formation, step 2. We do not propose that the chemisorbed ethylene state behaves as an extrinsic precursor and therefore this functionality does not apply.

The rate constants for ethylene desorption and ethyl group formation indicate that $k_2 \gg k_{-1}$ at the δ_1 evolution temperature. Values of k_2/k_{-1} calculated at 220 K vary from approximately 10 to 20 depending on the value of A_2 chosen prior to optimization (section 3.5 and Table IV). It is clear that $r \approx k_1 c_{ethyl}$, and the activation energy of 13.2 kcal/mol is indicative of β-hydride elimination (Figure 7, Table II).

Table IV. Ab Initio Calculated Barriers (kcal/mol) to C_2H_4 + H Migratory Insertion and the Reverse β-Hydride Elimination in $M(H)_2(C_2H_4)(PH_3)$[99]

M	activation barriers		ΔH of insertion, kcal/mol
	insertion	elimination	
Ni	0.6	32.1	−31.5
Pd	8.0	11.0	−3.0
Pt	12.5	8.3	4.2

4. Discussion

4.1. Binding of Ethylene on Fe(100)–H. The binding energy for molecular ethylene on the hydrogen-saturated Fe(100) surface is 8.5 ± 2 kcal/mol. For metal surfaces other than Fe(100)–H the ethylene bonding energy is generally not known, since decomposition usually predominates,[14-30] and ethylene evolved during TPRS is often that which is destabilized at high adsorbate coverage or is displaced by decomposition products. In these cases a true $M-C_2H_4$ bond strength cannot be extracted. The bond energies relevant to this discussion are for active metals which have been precovered by hydrogen, but these are not available. However, the adsorption of ethylene on Ru(001) at 100 K is sharply reduced by preadsorbed H adatoms;[42] extrapolation to $\Theta_H = 1$ indicates that no ethylene would adsorb at this coverage. Hydrogen thus reduces the $Ru-C_2H_4$ bond energy below that needed to stably adsorb ethylene at 100 K. Ethylene desorption from the (110) surfaces of the relatively inert metals Cu, Ag, and Au is quite similar to that for Fe(100)–H. On Cu(110) C_2H_4 desorbs near 210 K, with an approximate surface bonding energy of 13 kcal/mol.[78] On Ag(110) and Au(110) C_2H_4 desorption occurs in a broad state between 100 and 200 K, indicative of a binding energy of roughly 10 kcal/mol.[79-81] Clearly the H adatoms passify the Fe surface substantially. The mode of bonding of ethylene on Fe(100)–H will soon be examined with use of vibrational spectroscopies in this laboratory.

4.2. Migratory Insertion and β-Hydride Elimination: Comparison to Complexes. In this section we compare ethylene–hydrogen insertion and ethyl β-hydride elimination reactions among surfaces, mononuclear complexes, and cluster complexes, placing the reactivity on hydrogen-covered Fe(100) within the context of both homogeneous and surface chemistry. However, only in the realm of mononuclear complexes are quantitative values for rate constants available for comparison with those we have obtained. We discuss the energetics for hydrogenation of ethylene with respect to binding energies and kinetic parameters. The

(74) Values for A_2 and E_2 were initially taken to reproduce the α desorption state at an intermediate heating rate of 3.4 deg K/s and needed to be adjusted only slightly in order to match the experimental T_p and $\Delta T_{1/2}$ of α desorption as A_{-1} and E_{-1} were varied. Adjustments finer than 0.5 in log (A_2) and 0.05 kcal/mol in E_2 were unnecessary in order to fit T_p and $\Delta T_{1/2}$ within experimental error. However, as noted above the slope and midpoint of the plot of $\delta_1/(\alpha + \delta_1)$ versus ln (β) were quite sensitive to estimated values of A_{-1} and E_{-1}, thus increments of 0.1 for log (A_{-1}) and 0.005 kcal for E_{-1} were used to obtain the fit to the plot in Figure 9.

(75) Sensitivity of the results to A_{-1} and E_{-1} are demonstrated by the poor match between the data and simulations (1) using a log (A_{-1}) value 1.0 higher than the optimum with an E_{-1} value selected to match the midpoint of the linear fit to the data (dashed line)) and (2) using the optimum A_{-1} with E_{-1} 0.05 kcal/mol higher than optimum (dotted line).

(76) Gorte, R.; Schmidt, L. D. *Surf. Sci.* **1978**, *76*, 559.

(77) King, D. A. *Surf. Sci.* **1977**, *64*, 43.

(78) Outka, D. A.; Friend, C. M.; Jorgensen, S.; Madix, R. J. *J. Am. Chem. Soc.* **1983**, *105*, 3468.

(79) Outka, D. A.; Madix, R. J. *J. Am. Chem. Soc.* **1987**, *109*, 1708.

(80) Barteau, M. A.; Madix, R. J. *Proc. ICSS-4, ECOSS-3, Cannes* **1980**, 448.

(81) Barteau, M. A.; Madix, R. J. *Surf. Sci.* **1981**, *103*, L171.

comparison of Fe(100) with metals in the three regimes is followed by a discussion of the specific reactivity of Fe(100).

The kinetics of migratory insertion of olefins into M–H bonds and the reverse step of β-hydride elimination have been the subject of only a few quantitative studies.[82-85] In homogeneous complexes these two steps often rapidly equilibrate, making kinetic analysis extremely difficult. The kinetics may also be coupled with other reaction steps, such as the loss of ligands to achieve the coordinative unsaturation required for β-hydride elimination.[86-88] Similar reactivity patterns have been found in cluster complexes as well. In the hydrogenation of ethylene by $H_4Ru_4(CO)_{12}$,[10] insertion and β-hydride elimination steps have been inferred to be rapid, and at least the β-elimination step is taken to be fast in the isomerization of higher olefins by $H_2Os_3(CO)_{10}$.[89] In the case of surfaces these reaction steps have not yet been extensively studied.

There appear to be no experimental values of for β-hydride elimination for *typical* coordinatively unsaturated complexes, clusters, or surfaces to compare with our values for Fe(100). Due to the facile nature of the β-hydride elimination reaction for complexes with an alkyl cis to a vacant coordination site, the cases in which the reaction is slow enough for kinetics to be measured with standard techniques must be considered anomalies. Of three reactions reported where β-hydride elimination is the slow step in thermolysis; two, *trans*-$Pd(C_2H_5)_2(PPh_3)_2$[90] and $Ir(n\text{-}C_8H_{17})(CO)(PPh_3)_2$,[71] involve stable square-planar 16-electron complexes. There is thus a considerable energy involved in structural rearrangements to reach the quasitetrahedral transition state for β-hydride elimination.[91-93] The third example is the decomposition of $Co(C_2H_5)_2(acac)(PPhMe_2)_2$ (acac = acetylacetonato),[70] where rapid loss of a phosphine ligand preceeds the rate-determining step of β-hydride elimination; an activation energy of 30.6 kcal/mol and a preexponential of 10^{20} s^{-1} were measured for this reaction. For this species the large activation barrier is not as easily explained as for the Pd and Ir complexes, but some insight is gained from calculations for another coordinatively unsaturated d^6 complex, $HRh(C_2H_5)Cl(PH_3)_2$.[94] In this case a structural rearrangement of the complex whereby the alkyl migrates from its minimum energy position cis to the hydride into the trans position appears to be a major factor. Since this reaction is often so facile for complexes, our activation energy value of 13 kcal/mol for β-hydride elimination of C_2H_5 appears reasonable. Furthermore, the preexponential factor on Fe(100)-H of $10^{13.4}$ s^{-1} is a value expected for a cyclic transition state.

β-Hydride elimination has been studied qualitatively following the photolysis of ethyl chloride on Pt(111) to form surface ethyl groups.[67] Vibrational studies indicate that the ethyl groups are stable at 200 K but decompose via β-hydride elimination by 230 K to yield adsorbed ethylene. No kinetic parameters are available from this study, but the similarity in temperatures for β-hydride elimination on Pt(111)–Cl and Fe(100)–H suggests the rates may be quite similar on the two surfaces.

Olefin insertion into the M–H bond has been the subject of several detailed studies recently with the use of NMR, with which the rate of exchange between olefinic hydrogens and the hydride can be monitored on a time scale of 0.01.[83,85] Studies on $HRh(C_2H_4)(P\text{-}i\text{-}Pr_3)_2$ have yielded an activation energy and preexponential of 13.6 kcal/mol and $10^{12.8}$ s^{-1}, respectively, for the insertion process.[83] In the minimum energy configuration of the cis olefin hydride the C=C bond axis is normal to the equatorial plane. Similar, yet more detailed, experiments have been conducted on the migratory insertion of a variety of olefins in $NbH(Cp^*)_2(olefin)$.[85] The C=C bond in these Nb complexes is coplanar with the Nb–H axis. For ethylene insertion the activation energy of 15.3 kcal/mol and preexponential of $10^{10.8}$ s^{-1} are similar to those found for the Rh(I) complex mentioned above. The value of the activation energy for insertion calculated by Daniel et al. for $H_2RhCl(C_2H_4)(PH_3)_2$, a simplified model of Wilkinson's catalyst, was 18.4 kcal/mol.[94]

No accurate values are available for the kinetics of olefin migratory insertion into M–H bonds on metal surfaces. However, evidence that the processes are facile exists in the form of observed H–D exchange[14,29,30] and hydrogenation[27,28,30] of ethylene on several single-crystal surfaces (section 1). The activation energy of 6 ± 1 kcal/mol determined here for the migratory insertion of ethylene into the M–H bond on Fe(100)–H is remarkably lower than that found for complexes. In fact, the activation energy for ethyl group formation is very close to that expected for hydrogen diffusion on transition-metal surfaces.[95] The disparity in agreement between the kinetics of migratory insertion and β-hydride elimination on Fe(100)–H and mononuclear complexes probably originates in the complexity of these processes in transition-metal complexes.

Thorn and Hoffmann[91] and Fukui and Inagaki[96] have described the migratory insertion process in mononuclear transition-metal complexes in general terms which apply regardless of the coordination number and structure of the complex. They have concluded that the reaction is energetically unfavorable without the participation of an unoccupied metal d orbital which has lobes directed toward the cis hydride and olefin groups; these d orbital lobes are of opposite sign with respect to each other. If a given olefin hydride complex has the required electronic structure, the hydride and olefin must then bind cis to one another with the olefin C–C axis coplanar with the M–H bond axis. In addition, the olefin and hydride must be oriented with respect to other ligands so that they have the proper interaction symmetry with a vacant d orbital.[91] Activation barriers result from the rearrangements in the complex that are necessary to formation of this orientation, and they can be considerable. For square-planar d^8 Pt complexes the barrier to rotation of ethylene about the metal–olefin axis has been determined experimentally and theoretically to be approximately 15 kcal.[97] Calculations performed for the rotation of ethylene in complexes of varying coordination numbers by Hoffmann and co-workers show that values similar to this result when the ligand sphere is uncrowded and the ligand geometry is allowed to relax during the process. However, if ligand reorganization is not possible, as may be the case for bulky ligands, the barrier could be much higher; for $Fe(CO)_4(C_2H_4)$ with rigid CO ligands[98] the ethylene rotational barrier was calculated to be 32 kcal/mol.

Comparing the reaction barrier on Fe(100)–H to that of complexes thus requires a separation of the rearrangement energy, and this is best done in calculations where the proper reaction configuration is used for the initial state of the reactants. In this case the barrier for migratory insertion of ethylene into the M–H bond of several d^8 complexes of Ni, Pd, and Pt has been found to be either low, e.g. 7 kcal for $Pd(H)_2(C_2H_4)(PH_3)$ and 12 kcal for the Pt analogue,[99] or virtually nonexistent, e.g. for $Ni(H)_2(C_2H_4)(PH_3)$ and $PtHCl(C_2H_4)(PH_3)_2$.[99,91,92] The barrier for the

(82) Cross, R. J. In *The Chemistry of the Metal–Carbon Bond*; Hartley, F. R., Patai, S., Eds.; Wiley: New York, 1985; Vol. 2.
(83) Roe, D. C. *J. Am. Chem. Soc.* **1983**, *105*, 7770.
(84) Bercaw, J. E. In *Organometallic Compounds*; Shapiro, B. L., Ed.; Texas A&M Press: College Station, TX, 1983.
(85) Doherty, N. M.; Bercaw, J. E. *J. Am. Chem. Soc.* **1985**, *107*, 2670.
(86) Whitesides, G. M.; Gaasch, J. F.; Stedronsky, E. R. *J. Am. Chem. Soc.* **1972**, *94*, 5258.
(87) Reger, D. L.; Culbertson, E. C. *J. Am. Chem. Soc.* **1976**, *98*, 2789.
(88) Kurosawa, H.; Majima, T.; Asada, N. *J. Am. Chem. Soc.* **1980**, *102*, 4948.
(89) Deeming, A. J.; Hasso, S. *J. Organomet. Chem.* **1976**, *114*, 313.
(90) Ozawa, F.; Ito, T.; Yamamoto, A. *J. Am. Chem. Soc.* **1980**, *102*, 6457.
(91) Thorn, D. L.; Hoffmann, R. *J. Am. Chem. Soc.* **1978**, *100*, 2079.
(92) Sakaki, S.; Kato, H.; Kanai, H.; Tarama, K. *Bull. Chem. Soc. Jpn.* **1975**, *48*, 813.
(93) Reference 5, Chapter 2.
(94) Daniel, C.; Koga, N.; Fu, X. Y.; Morokuma, K. *J. Am. Chem. Soc.* **1988**, *110*, 3773.
(95) Seebauer, E. G.; Kong, A. C. F.; Schmidt, L. D. *J. Chem. Phys.* **1988**, *88*, 6597.
(96) Fukui, K.; Inagaki, S. *J. Am. Chem. Soc.* **1975**, *97*, 4445.
(97) Hay, P. J. *J. Am. Chem. Soc.* **1981**, *103*, 1390.
(98) Albright, T. A.; Hoffmann, R.; Thibeault, J. C.; Thorn, D. C. *J. Am. Chem. Soc.* **1979**, *101*, 3801.
(99) Koga, N.; Morokuma, K. In *Quantum Chemistry: The Challenge of Transition Metals and Coordination Chemistry*; Veillard, A., Ed.; Reidel: New York, 1986.

Pd complex provides the best comparison with that for Fe(100)-H since the enthalpy change of insertion for the Pd complex (-3 kcal/mol) most closely approximates that for Fe(100)-H (-7 kcal/mol). From this viewpoint the activation barrier in complexes may be quite close to the 6 kcal/mol barrier on the Fe(100)-H surface. This indicates that the intrinsic barrier height (i.e. the kinetic barrier if the reaction is thermoneutral) for these reactions on surfaces and in complexes may be quite similar when energies of structural rearrangement are removed from the activation barrier in the complexes.

5. Conclusions

Ethylene adsorbs molecularly on hydrogen-presaturated Fe(100) and undergoes a migratory insertion reaction to form stable ethyl groups. No ethane is formed and no ethylene decomposes on this surface. The insertion reaction proceeds with a preexponential of $10^{8\pm2}$ s^{-1} and an activation energy of 6 ± 1.5 kcal/mol. Competing with ethyl formation is molecular desorption of ethylene, with an activation barrier of 8 ± 2 kcal/mol and a preexponential of $10^{11\pm2}$ s^{-1}. Ethyl groups undergo β-hydride elimination with rate parameters of 13.2 kcal/mol and $10^{13.4}$ s^{-1} for E and A, respectively. Reversible migratory insertion and β-hydride elimination are responsible for multiple H-D exchange for C_2H_4 on a deuterium-covered surface.

Comparison of our results to those for transition-metal complexes indicates that the activation energies for migratory insertion and β-hydride elimination on Fe(100) correlate well with theoretical values for complexes when energetics of ligand rearrangement in complexes are separated.

Acknowledgment. This work was supported by the National Science Foundation (NSFCHE86-15910 and NSFCHE89-19406). M.L.B. also gratefully acknowledges support by a National Science Foundation Graduate Fellowship.

Rate Law and Activation Energy of Isotope Mixing between Chemisorbed CO Molecules on a K-Promoted Ni(111) Surface

Kumar Sinniah, William D. Sands, John T. Yates, Jr., and Kenneth C. Janda*

Contribution from the Department of Chemistry and Surface Science Center, University of Pittsburgh, Pittsburgh, Pennsylvania 15260. *Received October 24, 1990. Revised Manuscript Received February 1, 1991*

Abstract: Laser induced thermal desorption measurements are used to measure the kinetics of isotope exchange between CO molecules chemisorbed on a potassium-promoted Ni(111) surface: $^{13}C^{16}O + {}^{12}C^{18}O \rightleftharpoons {}^{13}C^{18}O + {}^{12}C^{16}O$. The efficiency of the reaction is maximized for a 1:1 K:CO stoichiometry and a 0.3 adspecies/Ni ratio for both K and CO. Over the temperature range 400–525 K the isotope exchange reaction has an apparent activation energy of only 72 ± 4 kJ/mol. Even for long reaction times and high surface temperature, however, the reaction proceeds to only 50% of the statistical limit. To explain these phenomena, we propose that the reaction proceeds via a $K_2C_2O_2$ etherate intermediate adsorbed on Ni(111). This species may be of importance in the promoter action of potassium on CO chemistry on transition-metal surfaces.

Introduction

Activation of the C–O bond in chemisorbed carbon monoxide is one of the most widely studied problems in surface science, yet the primary steps of CO activation are still not well understood at a fundamental level. Several recent reviews highlight the vast body of data on the efficiency of various metallic combinations as catalytic systems.[1] A particularly interesting model system for the heterogeneous catalytic activation of CO is a single-crystal Ni(111) surface promoted by potassium. Although the CO/K/Ni system has received much attention over the past decade, the mechanism for CO bond activation on this important model system has yet to be determined.[1]

CO is relatively unreactive on a clean Ni(111) surface. It bonds to the surface molecularly as terminal and bridge CO species, depending on coverage, and desorbs when the surface is heated to 430 K. CO-stretching frequencies measured by IRAS (infrared reflection absorption spectroscopy) provide a measure of the CO–surface interaction. At full coverage, terminally bonded CO exhibits a CO frequency of 2058 cm^{-1}; bridge-bonded CO exhibits a frequency of 1914 cm^{-1}.[2] These frequencies may be compared to 2143 cm^{-1} for the gas-phase molecule.[3] The bonding of CO on Ni changes dramatically as potassium is added to the surface. The CO vibrational frequency is strongly dependent on the magnitude of both the CO and K coverage.[4] At high K coverages, the CO vibrational frequency drops to near 1400 cm^{-1}, and the CO desorption temperature increases to 640 K.[4] Evidence from metastable quenching spectroscopy suggests that the CO adsorbed at the site with a ~1400-cm^{-1} frequency is nearly parallel with the surface, but the detailed structure is not known.[5] Several different K–CO complexes on different transition-metal surfaces have been proposed, but no conclusive evidence has been presented to support any particular model for the CO/K/Ni system.[5-8]

Another measure of the extent of interaction of CO with the surface is the occurrence of isotope mixing between adjacent CO molecules (i.e. $^{12}C^{18}O + {}^{13}C^{16}O \rightarrow {}^{12}C^{16}O + {}^{13}C^{18}O$). This reaction is especially interesting because it involves complete cleavage of the original CO bonds to make new ones. Ng et al.[9] have shown that this reaction does not proceed with an observable rate on clean Ni(111) in agreement with earlier studies on Ni(100).[10] It has been shown by Ng et al.[9] and Lee et al.[11] that

(1) *Physics and Chemistry of Alkali Metal Adsorption*; Bonzel, H. P., Bradshaw, A. M., Ertl, G., Eds.; Elsevier: New York, 1989. Bonzel, H. P. *Surf. Sci. Rpt.* **1987**, *8*, 43. Heskett, D. *Surf. Sci.* **1988**, *199*, 67.
(2) Surnev, L.; Xu, Z.; Yates, J. T., Jr. *Surf. Sci.* **1988**, *201*, 1, 14, and references therein.
(3) Huber, K. P.; Herzberg, G. *Constants for Diatomic Molecules*, Van Nostrand Reinhold: New York, 1979.
(4) Uram, K. J.; Ng, L.; Yates, J. T., Jr. *Surf. Sci.* **1986**, *177*, 253. Uram, K. J.; Ng, L.; Folman, M.; Yates, J. T., Jr. *J. Chem. Phys.* **1986**, *84*, 2891.
(5) Arias, J.; Lee, J.; Dunaway, J.; Martin, R. M.; Metiu, H. *Surf. Sci.* **1985**, *159*, L433.
(6) dePaola, R. A.; Hrbek, J.; Hoffmann, F. M. *J. Chem. Phys.* **1985**, *82*, 2484.
(7) Lackey, D.; Surman, M.; Jacobs, S.; Grider, D.; King, D. A. *Surf. Sci.* **1985**, *152/153*, 513.
(8) Solymosi, F.; Berko, A. *Surf. Sci.* **1988**, *201*, 361.
(9) Ng, L.; Uram, K. J.; Xu, Z.; Jones, P. L.; Yates, J. T., Jr. *J. Chem. Phys.* **1987**, *86*, 6523.
(10) Goodman, D. W.; Yates, J. T., Jr. *J. Catal.* **1983**, *82*, 255.
(11) Lee, J.; Arias, J.; Hanrahan, C. P.; Martin, R. M.; Metiu, H. *J. Chem. Phys.* **1985**, *82*, 485.

0002-7863/91/1513-3684$02.50/0